ISSN 1 746-7233, England, UK
World Journal of Modelling and Simulation
Vol. 12 (2016) No. 4, pp. 243-258

Torque transmitted by the nematic liquid crystal to the faceted nanoparticles

Shivkumar Bale[1]*

Cain Department of Chemical Engineering, Louisiana State University, Baton Rouge, LA 70803, U.S.A.

(*Received December 21 2015, Accepted June 27 2016*)

Abstract. We investigated the torque that develops when faceted nanoparticles, namely cubes and triangular prisms, are immersed in a nematic LC. We used a mesoscale theory in terms of tensor order parameter $Q(r)$ to model the nematic. Homeotropic anchoring condition of the NLC is imposed on the surfaces of faceted nanoparticles. Our results indicate that, when the faceted particle is oriented at an out-of-plane orientation (i.e. unstable configuration), it moves away immediately from that state and then slowly orients itself back to the stable configuration (i.e. in-plane orientation). The magnitude of out-of-plane torques is similar to that of in-plane torques. In the case of an isolated nanoprism system, the torque reaches maximum when the particle orients with one of its rectangular sides parallel to the far field director $n(r)$. In contrast, for an isolated nanocube system, the torque reaches maximum when the particle orients with its four lateral faces parallel to the far field director $n(r)$. This computational study would be relevant to the switching studies by external means.

Keywords: nanoparticles, liquid crystals, torque, faceted, homeotropic anchoring

1 Introduction

Systems of particles immersed in LCs have attracted attention for the development of composite and structured materials. When the particles are introduced in the LC, they produce a distortion in its director field. Thus the particles and the LC will try to minimize the elastic perturbation, which leads to long range interparticle interactions. These interactions can induce the formation of a number of ordered colloid structures[27, 33, 39, 40, 42, 43, 46–48, 52, 56–59, 64, 67, 68] and depends on the shape and the size of the particles, the local anchoring of the LC at the surface of the colloids, the alignment of the director field far away from the particles, and the geometry of the surrounding. According to recent experiments[33, 39, 42, 43, 46–48, 52, 56–58, 62, 64, 67, 68] and calculations[15, 17, 18, 22, 23, 26, 39, 42, 43, 52, 56–58, 64], long-range interparticle interactions are anisotropic and can be as strong as several thousands of kBT. Most of the above experimental work has considered systems of spherical, micron sized particles in LC; however, a number of experimental studies have worked on spherical[28, 38, 41, 49, 51, 65] or rod-like nanoparticles[7, 8, 19, 31, 34, 35, 50] in LC. The principle behind the use of LCs to organize particles of spherical and rod-like shapes can be extended, in principle, to particles with shapes other than spherical, as well as particles with anisotropic surface patterns. This will lead to the formation of ordered particle structures with unusual morphologies different from the conventional hexagonal close-packed crystals formed by spherical colloids[12–14, 25, 55, 66]. A number of applications, e.g. in colloidal crystals, photonics, nanoscale electronics, memory storage, light-scattering devices, electro-optical switches and displays, are envisioned for these unusually-ordered particle arrays. Recently, thermodynamic properties such as LC defect structures and potentials of mean force for faceted particles, namely cubes[3, 61] and triangular prisms[6, 36], have been determined [21]. It was observed that several properties of the particles (e.g., shape, size) affect the strength and the anisotropy of the LC-mediated interparticle interactions. The morphology and the thermodynamic stability of

* Corresponding author. *E-mail address*: sbale1@lsu.edu

the structures that could be assembled from these particles were predicted. Phillips, et al analyzed the defect textures in the polygonal arrangement of faceted nanoparticles in the nematic LC as a function of temperature, polygon size, and polygon number[45]. It was observed that the bulk defects were favored at high temperatures and small polygon size, whereas the surface defects were favored at low temperatures and large polygon size. With increasing number of polygons, according to Zimmer's texture rule, the central defects increases at high temperatures, whereas at lower temperatures, the number of surface defects increases. It was reported that the unusually-ordered particle assemblies could be used to form metamaterials which is used for cloaking devices or light-based circuits[60]. In order to engineer a metamaterial, the self assembly of complex anisotropic colloids requires to be manipulated and their orientations should also be controlled[32].

Recently, several researchers studied torques on the colloids in nematic host fluid. Dontabhaktuni, et al calculated torques on individual triangular, square and pentagonal sub-micrometer sized platelets in a thin layer of nematic liquid crystal by using 3D numerical modeling, which is important for switching applications 8. It was observed that the platelets with quadrupolar symmetry are orientationally, more strongly bounded than the platelets with dipolar symmetry. Lapointe, et al investigated the rotational dynamics of square platelet colloids in nematic LC around multiaxis due to the application of external electric field[32]. It was demonstrated that the square platelet colloids in nematic LC can be rotated around multiple rotational axis even for a fixed direction of the applied field. Senyuk, et al investigated the elastic pair interaction forces, torques and binding energies between colloidal particles with dissimilar shapes and dimensions in nematic liquid crystals[54]. This study exhibited behavior such as omnidirectional attraction, which is not observed in monodisperse colliodals in LCs. Tao, et al studied the dynamics of ZnO nanowires in an in-plane switching 5CB liquid crystal cell, both numerically and experimentally[63]. It was observed that in a nematic phase, there are two factors that control the relaxation and the response of the ZnO nanowires. The first factor is the dielectrophoretic torque induced by the applied electric field and the second one is the elastic torque exerted by the liquid crystals. Rovner, et al studied torques on a colloidal disk with homeotropic surface anchoring in a nematic liquid crystal cell [53]. It was found that the normal to the colloidal disk, in the absence of magnetic field, faces parallel to the nematic director. Whereas, when the magnetic field is applied, the colloidal disk rotates such that the magnetic torque and the elastic torque due to the distortion of the nematic director field are balanced.

When a particle is immersed in LC, the alignment of the LC is distorted because of the anchoring condition of the LC at the surface of the particle. Due to this distortion in the LC profile, the LC is expected to transmit torques to the particle in order to minimize its distortion around the particle. If the alignment of the LC is "switched" by external means, the particle will try to reorient back to the stable configuration. Our objective is to analyze the reorientational behavior of a faceted particle which would be relevant to the switching studies by external means. Thus, we computed restoring torques transmitted by NLC to the faceted particle. We concentrated specifically on several faceted nanoparticles, namely cubes[3, 61] and triangular prisms[6, 36]. Since we are interested in the interparticle interactions and arrangements, the LC does not need to be modeled at the atomic level of detail. Rather, the LC in this part of the project is modeled using a mesoscale theory in terms of the LC tensor order parameter Q[5], which can allow the study of larger system sizes. Computer simulations will be key in this study to systematically explore and quickly predict the behavior of the systems, aiming at influencing future experimental efforts.

2 Models and methods

2.1 Details of the model systems

The system considered here is a rectangular box full of nematic LC with dimensions L_x, L_y and L_z, containing one or two particles. A schematic representation of the rectangular box filled with nematic is shown in Fig. 1(a). Periodic boundary conditions are applied to the system in x and y direction. The system is covered with walls at top and bottom which provides homeotropic (perpendicular) anchoring to the nematic LCs. Nematic LCs also have homeotropic anchoring at the surface of the particles. This anchoring is easy to achieve experimentally by coating the surfaces with self-assembled monolayers of alkanethiols[16]. When there are no particles in the system, the nematic LC aligns its director field parallel to the z axis. The alignment

of the nematic LC is distorted when a particle is introduced in the system because the orientation of the LC far away from the particle does not match with the orientation of the LC around the particle. This mismatch occurs due to the homeotropic anchoring of the LC at the surface of the particle and leads to the formation of topological defects.

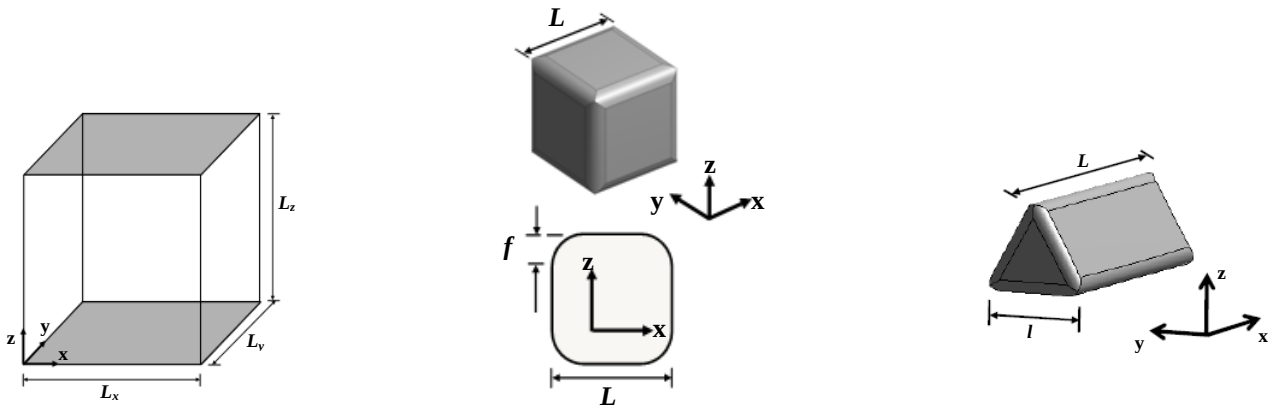

(a) (b) (c)

Fig. 1: Schematic representation of (a) rectangular box full of nematic liquid crystal, (b) cubic nanoparticle, and (c) equilateral triangular prism shaped nanoparticle [21]

In our research, we studied cube and triangular prism shaped nanoparticles with rounded edges. The cubic particle has sides with length $L = 40$ nm and rounded edges $f = 5$ nm (Fig. 1(b)) whereas the equilateral triangular prism shaped particle has rectangular faces with length $L = 150$ nm, triangular faces with length $l = 68.7$ nm and rounded edges $f = 5$ nm (Fig. 1(c)). We studied one- and two-particle systems in our calculations. For one cubic particle systems, the cube has its center of mass placed in the centre of the nematic cell. The cubic particle is rotated around five out of thirteen rotational symmetry axes: (1) x axis (2) $x = y = z$ axis (3) $x = 0, y = z$ axis (4) $y = 0, x = z$ axis and (5) $z = 0, x = y$ axis (Fig. 2(b)). Based on the octahedral symmetry of a cube and how this symmetry is broken by the presence of a distinguished direction [i.e. the far-field director $n(r)$, which is parallel to the z axis], rotations of the cubic particle around the other eight rotational symmetry axes will lead to configurations similar to those found for the five rotations described above. For two cubic particle systems, our research was limited to two cubic particles approaching each other, with each particle having a fixed orientation similar to the most stable configuration obtained from the one particle system. We considered two cubic particles approaching in such a way that the defects touch each other and their respective rounded edges are parallel to each other. The dimensions of the rectangular box for the one cubic particle system are $L_x = L_y = L_z = 100$ nm whereas the dimensions of the rectangular box for the two cubic particle system are $L_x = 130$ nm, $L_y = 190$ nm and $L_z = 120$ nm.

For one triangular prism system, the particle has its center of mass placed in the center of the nematic cell. The triangular prism particle is rotated around two axes (1) x axis and (2) the axis passing through two diagonal vertices of the triangular faces (Fig. 2(a)). During these rotations, the longest side of the particle is perpendicular to the far field director. We did not rotate the triangular prism particle around the y axis because rotating the particle around the y axis will cause the longest side of the particle to become parallel to the far-field director; when the longest side of the particle becomes parallel to the far-field director, we have large free energy penalty according to the research for the system of one spherocylindrical particle in the nematic LCs[23]. Triangular prism particle can be rotated around many axes but it was rotated around the above mentioned two axes because it will lead to configurations similar to those found for the remaining other rotations, since the far field director is parallel to z-axis. For two triangular prism particle systems, we limited our research to two particles approaching each other, with each particle having configuration similar to the stable configuration obtained from the system of one particle. Depending upon the PMF results obtained from one triangular prism particle system[21], the triangular nanoprisms can be the building blocks of several ordered

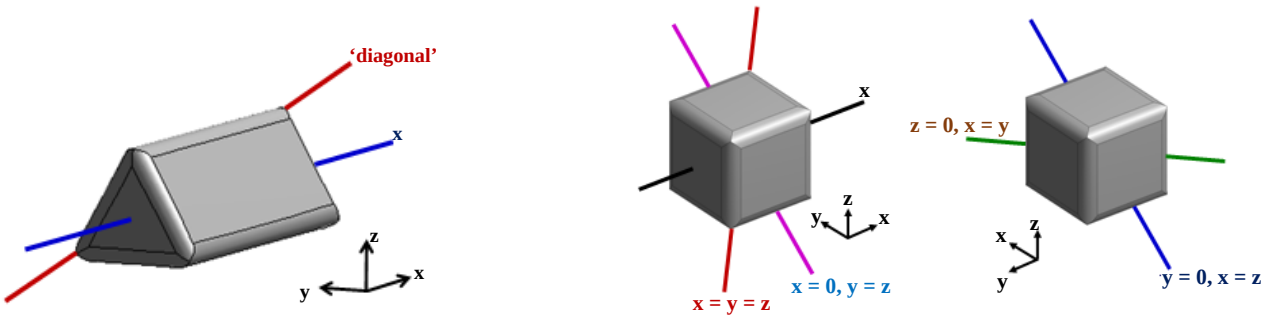

(a) (b)

Fig. 2: (a) The triangular prism particle is rotated around the two axes (1) only x axes (2) the axis passing through two diagonal vertices of two triangular faces as indicated in the Fig.. In all cases, far field director n(r) is parallel to the z-axis. (b) The cubic nanoparticle is rotated around the five axes out of thirteen rotational symmetry axes as indicated in the Fig.

arrays where the particles have their longest side rotated along x axis but their centers placed on different axes; their orientation may also vary. As a result, three ordered arrays of two nanoprisms were considered (1) centers are on x axis and both the particles have the same orientation (linear array) (2) centers are on y axis and both the particles have the same orientation (parallel array) and (3) centers are on y axis, with one of the particle inverted with respect to the other one (inverted parallel array). Out of three ordered arrays, according to the PMF and defect structure results[21], inverted parallel array was found to be thermodynamically more stable than the linear and parallel array. Therefore, torques for only inverted parallel array was calculated. The dimensions of the rectangular box for the one triangular prism particle system are $L_x = L_z = 1000$ nm, $Ly = 500$ nm. The dimensions of the rectangular box for the two triangular prism particle system are $L_x = 400$ nm, $L_y = 1200$ nm and $L_z = 300$ nm for inverted parallel array.

For one particle system, as a faceted particle is rotated in the nematic cell along a particular direction, there is a change in the nematic profile which applies restoring torque to the particle. In one particle system, restoring torques depends on the angle of rotation θ along a particular direction. When several particles are immersed in the LC, the reorientational behavior of a faceted particle depends on the restoring torque applied on each particle and its interaction with the neighboring particles. Therefore, torques for two particle system is calculated. For two particle system, two particles are drawn closer to one another while keeping their orientation unchanged. Since the centers of such particles appear to glide along parallel, but non-coincident planes, one would expect that the torque they exchange through the intervening liquid crystal should make them turn. Keeping the particle's orientation unchanged amounts to apply restoring torques to both of them, which depends on the interparticle separation d.

2.2 Mesoscale theory for the nematic liquid crystal

The nematic LC is modeled using a mesoscale theory in terms of tensor order parameter $\boldsymbol{Q}(\boldsymbol{r})$. The tensor order parameter $\boldsymbol{Q}(\boldsymbol{r})$ is different from director field $\boldsymbol{n}(\boldsymbol{r})$ because it is free of discontinuities even at the LC defect core. The scalar order parameter $\boldsymbol{S}(\boldsymbol{r})$ and the director field $\boldsymbol{n}(\boldsymbol{r})$ can be calculated from $\boldsymbol{Q}(\boldsymbol{r})$ by using its largest eigenvalue 2S/3 and eigenvector[5]. In a recent study of spherical particles[15, 17, 18, 26], the nematic LC was modeled using this mesoscale theory and the results were compared with molecular simulations where the nematic was modeled using Gay-Berne ellipsoids. It was found that the results in both the cases were in agreement down to the nm-scales, which shows the validity of the mesoscale theory at these scales. The mesoscale theory also corresponds to the particular case of Beris-Edwards formulation[1]. According to this formulation, the evolution of tensor order parameter $\boldsymbol{Q}$ as a function of position $\boldsymbol{r}$ and time t is determined by the functional derivative of free energy of the liquid crystal F with respect to tensor order parameter $\boldsymbol{Q}$.

$$\frac{\partial \boldsymbol{Q}}{\partial t} = -\frac{1}{\gamma}\left[\frac{\delta F}{\delta \boldsymbol{Q}} - \frac{1}{3}\mathrm{Tr}\left(\frac{\delta \mathrm{F}}{\delta \boldsymbol{Q}}\right)\boldsymbol{I}\right], \tag{1}$$

where γ is the kinetic coefficient associated with the rotational viscosity of the liquid crystal and it is assumed constant. The functional derivative of the free energy of the liquid crystal F with respect to tensor order parameter Q is assumed to be symmetrized in Eq. (1). The following equation represents the free energy of the nematic liquid crystal and it is divided into three parts.

$$F = \int d\boldsymbol{r} f_{LdG}(\boldsymbol{r}) + \int d\boldsymbol{r} f_e(\boldsymbol{r}) + \oint dS f_s(\boldsymbol{r}). \tag{2}$$

The first term is Landau-de Gennes[5] expansion representing the short range interactions that drive the bulk isotropic to nematic phase transition.

$$f_{LdG} = \frac{A}{2}\left(1 - \frac{U}{3}\right)\mathrm{Tr}\left(\boldsymbol{Q}^2\right) - \frac{AU}{3}\mathrm{Tr}\left(\boldsymbol{Q}^3\right) + \frac{AU}{4}\left[\mathrm{Tr}\left(\boldsymbol{Q}^2\right)\right]^2. \tag{3}$$

A and U are the constants in the above equation which depends on the liquid crystal. A represents the energy scale of the model and U governs the bulk scalar order parameter

$$S_{bulk} = \frac{1}{4}\left(1 + 3\sqrt{1 - \frac{8}{3U}}\right). \tag{4}$$

When $0 < U < 2.7$, the system is isotropic but at $U > 2.7$, the system is nematic. $U = 3$ and $8/3$ are the metastability limit for isotropic and nematic phase respectively. The third term in Eq. (2) represents the contribution of surface to the free energy of the liquid crystal and accounts for anchoring of the liquid crystal at the surface of the particle. We are concerned with the limit of the infinitely strong homeotropic anchoring of the liquid crystal at the surface of the particle. The prescribed homeotropic anchoring of the liquid crystal at the surface should be satisfied at the limiting case otherwise the term f_s diverges. The homeotropic anchoring of the liquid crystal is applied at the surface through boundary conditions for calculation purposes.

The second term in Eq. (2) is the contribution of the long range elastic forces of the liquid crystal to the free energy and introduces a free energy penalty related to the gradients of the tensor order parameter field. In our research, we used one elastic constant approximation[5] where the constants K11 (splay), K22 (twist) and K33 (bend) have common value. During a recent study of spherocylindrical particles in a nematic liquid crystal[23], it was found that the results obtained from the one elastic constant approximation were similar to those from the three elastic constant approximation[1, 10, 11]. The term f_e in the Eq. (2) is as follows:

$$f_e = \frac{L_1}{2}\frac{\partial Q_{ij}}{\partial x_k}\frac{\partial Q_{ij}}{\partial x_k}. \tag{5}$$

In the above equation, $i, j, k \in x, y, z$, the Einstein summation convention over the repeated indices is used. When the Eq. (1) is evaluated using Eq. (2), (3) and (5), we obtain the set of partial differential equations of Q as follows:

$$\frac{\partial Q_{ij}}{\partial t} = -\frac{1}{\gamma}\left\{A\left(1 - \frac{U}{3}\right)Q_{ij} - AU\left[Q_{ik}Q_{kj} - \frac{\delta_{ij}}{3}Q_{kl}Q_{kl} - Q_{ij}\left(Q_{kl}Q_{kl}\right)\right] - L_1\frac{\partial}{\partial x_k}\left(\frac{\partial Q_{ij}}{\partial x_k}\right)\right\}. \tag{6}$$

The above equation gives the set of partial differential equations of Q which is solved numerically for all the systems in our study. The dimensionless constants are $A = 1$, $U = 6$, $\gamma = 400$ and $L_1 = 1$, corresponding to $S(bulk) = 0.81$. These parameters correspond to the elastic constant $K = 5$ pN (one elastic constant approximation) and viscosity $= 0.04$ Pa.s using the scaling factors for pressure (105 Pa), length (10 nm) and time (1 ns). These values of constants represent a low molecular weight liquid crystal like 5CB. For dimensional analysis, we can obtain a characteristics length scale (ξ) for the spatial variation of Q. The characteristics length scale (ξ) is equal to 17.3 for calculation purpose and its equation is presented as follows:

$$\xi = \sqrt{18L_1/AU}. \tag{7}$$

Since Q is traceless, it has five independent components of tensor order parameter Q (Q_{xx}, Q_{yy}, Q_{xy}, Q_{xz} and Q_{yz}). In order to obtain these components, Eq. (6) was solved by using finite elements and the COMSOL multiphysics package[4]. We used the time-dependent algorithm DASPK, combined with the linear system solver GMRES and the incomplete LU preconditioner[4] to solve all the equations. In order to minimize the free energy, the Eq. (6) is solved for sufficiently long period of time until the solution has almost no numerical variation. According to our previous studies[20, 22, 23], we carried out the simulation using unstructured meshes containing tetrahedral, linear Lagrange elements set as default mesh by COMSOL Multiphysics 44. Several grid densities were used in order to make numerical solution mesh independent. Mesh was finer near the wall and the nanoparticle, where the variation of Q is strong and curvature effects are present. For cubic particles, the minimum length of the finite elements in our finest grid size is $\sim 1.1 \times 10^{-4} L$ which is comparable to those reported by Fukuda et al[24]. The initial conditions of Q for the simulation are scalar order parameter $S(r)$ equal to $S(\text{bulk})$ and the director field aligned along the z direction. It was found that the results are similar when the calculations are started from the LC in an isotropic phase. The scalar order parameter at the surface of the particle was also set to $S(\text{bulk}) = 0.81$. We can visualize the distortion in the alignment of nematic LC by using different methods[2, 29, 30]. According to previous studies[15, 17, 18, 20, 22, 23, 26], we use the contour $S = 0.30$ to visualize the distortion because $S = 0.30$ is the lowest possible value of the scalar order parameter for the stable nematic LC in our model[1]. The torque T is calculated by the following equation[37].

$$T = \oint L v dS, \tag{8}$$

where v is the vector of normals acting on the surface of the particles and L is the couple stress tensor. The equation for L is given as follows

$$L_{ij} = 2\varepsilon_{ikl} Q_{km} \frac{\partial f}{\partial(\partial Q_{ml}/\partial x_j)}, \tag{9}$$

where ε is the Ricci's alternator and f is the free energy of the system, which includes Landau de Gennes expansion and long range elastic forces of liquid crystal (Eq. (2)). The three components of torque are calculated by numerical integration of Eq. (8) and (9) over the surface of the particles.

3 Results and discussions

3.1 Triangular prism shaped particle

3.1.1 Triangular prism shaped particle rotated around x axis

The total torque transmitted by the NLC on one triangular prism shaped nanoparticle, rotated around the x axis, as a function of angle of rotation is shown in Fig. 3. 3D visualizations of the NLC distortion around one triangular prism shaped particle are shown in Fig. 4. Torque profile for one faceted nanoparticle in NLC is mostly divided into in-plane and out-of-plane torques[9]. When a triangular prism shaped particle is rotated around the x-axis, the in-plane torque is observed, as the angle of rotation increases from the stable configuration ($\theta \sim 0^\circ$) to $\theta \sim 20^\circ$, because the torque transmitted by the NLC to the particle increases (Fig. 3), as the NLC distortion around the particle increases (Fig. 4). Out-of-plane torque is observed, just as the angle of rotation increases from $\theta \sim 20^\circ$ to $\theta \sim 30^\circ$, due to the torque transmitted by the NLC to the particle decreases (Fig. 3), while at the same time the NLC distortion around the particle increases (Fig. 4). The magnitude of the out-of-plane torque is similar to that of the in-plane torque, but varies more with respect to the angle of rotation, which is evident by its large slope (Fig. 3). According to our previous work[21], the isolated triangular nanoprism prefers to orient with one of its rectangular sides perpendicular to the far field director $n(r)$ since the NLC distortion around the preferred orientation is the smallest. Therefore, the stable configuration occurs at fixed interval with $\theta \sim 0^\circ$ and 60° (Fig. 4). These stable configurations have zero torque in the torque profile (Fig. 3). When the particle orients with one of its rectangular sides parallel to the far field director $n(r)$ (i.e. out-of-plane orientations), the torque reaches maximum (see the blue region in Fig.

3 and the corresponding 3D visualization in Fig. 4) because the NLC around the particle is highly distorted (Fig. 4). These out-of-plane orientations are unstable configurations and when a particle is oriented at these configurations, it immediately moves away from that state, which is evident by the large slope of the blue region shown in the Fig. 3, and then it slowly reorients itself to the closest stable configuration.

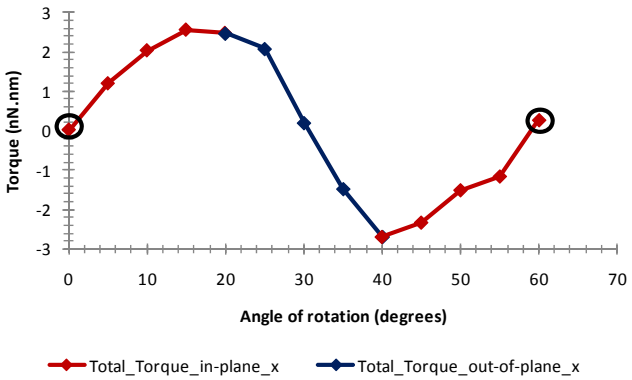

Fig. 3: Total torque transmitted by the nematic liquid crystal on the one equilateral triangular prism shaped nanoparticle, rotated around the x axis, as a function of angle of rotation. The blue region represents angles with out-of-plane rotation and the green region represents angles with in-plane rotation. Circles indicate the stable and zero torque configuration

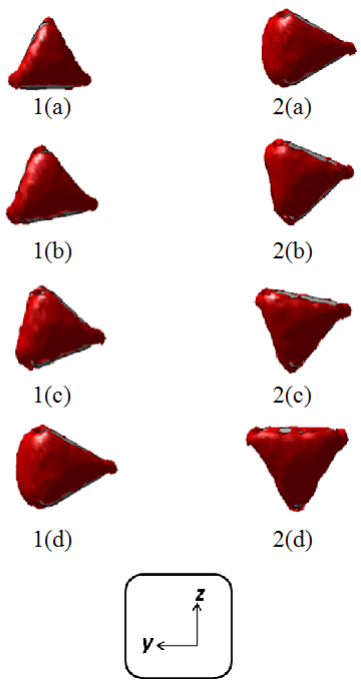

Fig. 4: 3D visualizations of the NLC distortion around the equilateral triangular prism shaped particle when the particle is rotated around x axis at angle θ

3.1.2 Two triangular prism shaped particle system

The x, y, and z components of the torque transmitted by the NLC to the triangular prism nanoparticles approaching each other along the $z-y$ plane is shown in Fig. 5. The schematic representation of two triangular

prism shaped particles approaching each other along the $z-y$ plane is shown in Fig. 6(a). Our results indicate that the x component of the torque transmitted by the NLC to the triangular prism particles ($T_{x(1,2)}$) varies significantly for the interparticle distances $d < 40$ nm whereas there is no variation in the magnitude of $T_{y(1,2)}$ and $T_{z(1,2)}$ for all the interparticle distances considered (Fig. 5). The torque $T_{x(1,2)} \sim 0$, when the triangular prism particles are separated by an interparticle distance $d > 40$ nm. However, while d is reduced, $T_{x(1,2)}$ increases, reaching a maximum value of ~ 3 nN.nm at $d \sim 10$ nm (Fig. 5). This positive torque in the x direction will rotate the triangular prism particles around their long axis in an anticlockwise direction. $T_{x(1,2)}$ shows positive torques with similar magnitude for $d < 40$ nm (Fig. 3). This behavior is observed because combining both the particles in an inverted parallel array leads to a parallelogram like structure (Fig. 6(b) and (c)). Since this structure behaves as a single particle and has its center on the y axis, it develops $T_{x(1,2)}$ with similar magnitude and direction. The magnitude of the torques transmitted by the NLC to the triangular prism particles can be reduced to some extent by allowing the particles follow a "diagonal" trajectory while approaching each other. Recently, Hung [20] observed that the magnitude of the torque $T_{x(1,2)}$ transmitted by the NLC to the long spherocylindrical particles decreased by 45%, when the particles approached each other via "diagonal" trajectory.

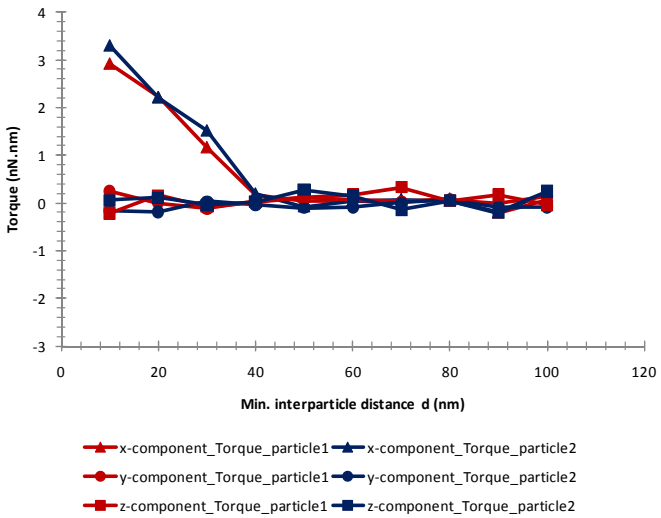

Fig. 5: Torque transmitted by the nematic liquid crystal on two equilateral triangular prism shaped particle system as a function of minimum surface-to-surface interparticle distance d. Triangles: x component of torque acting over particle 1 (red) and 2 (blue). Circles: y component of torque acting over particle 1 (red) and 2 (blue). Squares: z component of torque acting over particle 1 (red) and 2 (blue)

3.2 Cubic particle

The total torque transmitted by the NLC on the cubic nanoparticle rotated around the $y = 0$, $x = z$ axis is similar to that of rotated around the $x = 0$, $y = z$ axis. Therefore, the results for the torque transmitted by the NLC on the cubic nanoparticle rotated around the $y = 0$, $x = z$ axis are not presented. The total torque transmitted by the NLC on the cubic nanoparticle rotated around the $x = y = z$ axis, $x = 0$, $y = z$ axis, $z = 0$, $x = y$ axis and x axis is shown in Fig. 7 respectively. 3D visualizations of the NLC distortion around the cubic nanoparticle oriented at $\theta = 0°$, and at zero torque configuration along the four symmetry axes, as mentioned above, is shown in Fig. 8.

3.2.1 Cubic particle rotated around $x = y = z$ axis and $x = 0, y = z$ axis

When a cubic particle is rotated around the $x = y = z$ axis and $x = 0$, $y = z$ axis, the in-plane torque is observed, as the angle of rotation decreases from the zero torque configuration ($T = 0$) to $\theta \sim 30°$

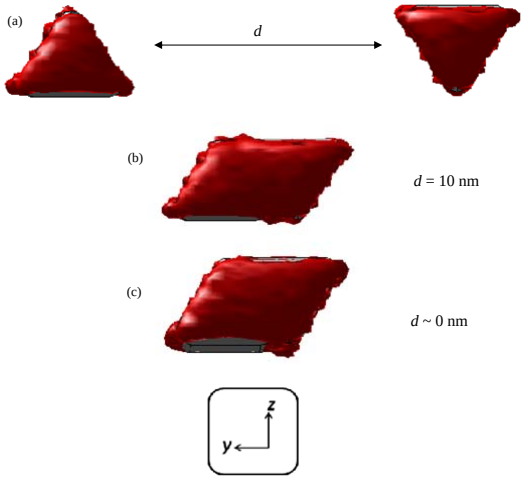

Fig. 6: (a) Schematic representation of two equilateral triangular prism shaped particles approaching each other through the interparticle distance d. (b) 3D visualizations of NLC distortion around two equilateral triangular prism shaped particles separated by the interparticle distance $d = 10$ nm (c) $d \sim 0$ nm

(Fig. 7), whereas the out-of-plane torque is observed, as the angle of rotation decreases from $\theta \sim 30^\circ$ to $\theta \sim 0^\circ$ (Fig. 7). According to our previous work[21], the isolated nanocube prefers to orient with none of its sides perpendicular to the far field director $n(r)$ since the NLC distortion around the preferred orientation is the smallest. Therefore, the particle has the most stable configuration at fixed interval with $\theta = 60^\circ$ for the $x = y = z$ axis and $\theta = 90^\circ$ for the $x = 0$, $y = z$ axis [21]. In order to have a zero torque, a configuration should have a high degree of symmetry along with a low NLC distortion around it. Thus, in the case of $x = y = z$ axis and $x = 0$, $y = z$ axis, the most stable configuration is also the zero torque configuration because of its high degree of symmetry (refer the corresponding 3D visualization in Fig. 8(c) and (d)). When a cubic particle orients with its four lateral faces parallel to the far field director $n(r)$ (i.e. out-of-plane orientations), the torque reaches maximum (see the blue region in Fig. 7, and the 3D visualization of NLC distortion around the maximum torque configuration in Fig. 8(a)), because the NLC around the particle is highly distorted. The magnitude of the in-plane torque is similar to that of the out-of-plane torque (Fig. 7). When a cubic particle is oriented around the $x = 0$, $y = z$ axis, the out-of-plane torque varies more with respect to the angle of rotation, as compared to that of the in-plane torque, due to the larger slope (Fig. 7). Hence, when a cubic particle is oriented at an unstable configuration (out-of-plane orientations), along the $x = 0$, $y = z$ axis, it moves away immediately from that state and then slowly reorients itself to the stable configuration (in-plane orientations). In the case of a cubic particle oriented around the $x = y = z$ axis, both the in-plane and the out-of-plane torques vary similarly with respect to the angle of rotation, due to the same slope (Fig. 7). Accordingly, for a cubic particle oriented at an unstable configuration along the $x = y = z$ axis, the movement of the particle from that state and then the reorientation to the stable configuration has the similar speed.

3.2.2 Cubic particle rotated around $z = 0, x = y$ axis

A cubic particle oriented along the $z = 0$, $x = y$ axis has a stable configuration at $\theta \sim 55^\circ$ and a zero torque configuration at $\theta = 90^\circ$ (see Fig. 7 and 3D visualization of NLC distortion around the zero torque configuration in Fig. 8(e)). The stable configuration along the $z = 0$, $x = y$ axis does not have a zero torque because of its asymmetry (refer [21]). When a cubic particle is rotated around the $z = 0$, $x = y$ axis, only the out-of-plane torque is observed, as the angle of rotation either increases or decreases from the stable configuration $\theta \sim 55^\circ$ (Fig. 7). However, just as the angle of rotation decreases from $\theta \sim 20^\circ$ to 0°, we observed an unconventional torque, instead of a small conventional positive (out-of-plane) torque, as a result of the rapid decrease in the NLC distortion around the particle over a small interval of the angle of rotation (refer [21] and 3D visualization in Fig. 9(a)). This odd effect might be due to the numerical error.

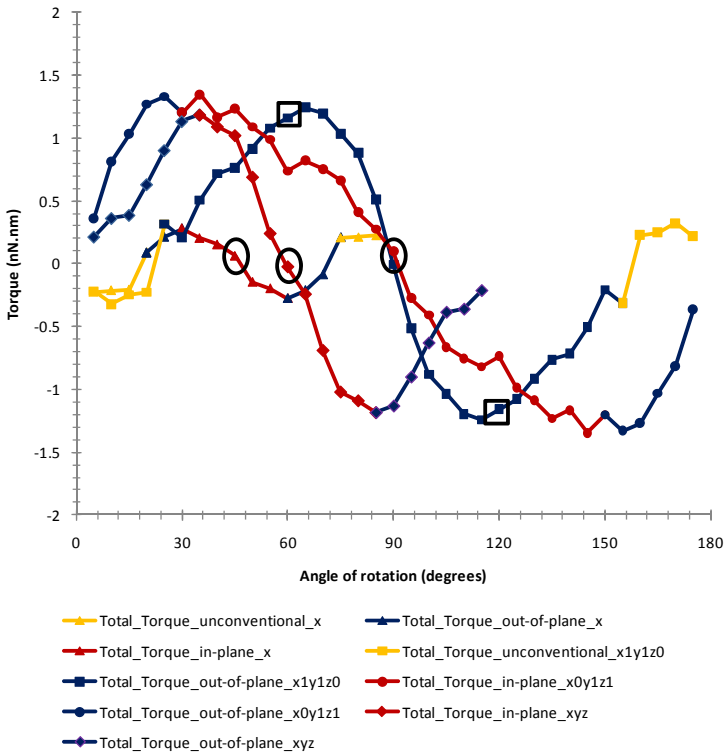

Fig. 7: Total torque transmitted by nematic liquid crystal on one cubic nanoparticle, rotated around the following symmetry axes: (triangle) the x axis; (diamond) the axis $x = y = z$; (circle) the axis $x = 0$, $y = z$; and (square) the axis $z = 0$, $x = y$, as a function of angle of rotation. The blue region represents angles with out-of-plane rotation, the red region represents angles with in-plane rotation and the black region represents angles with unconventional rotation. The enclosed circle indicates the zero torque configuration and the enclosed rectangle indicates the most stable configuration.

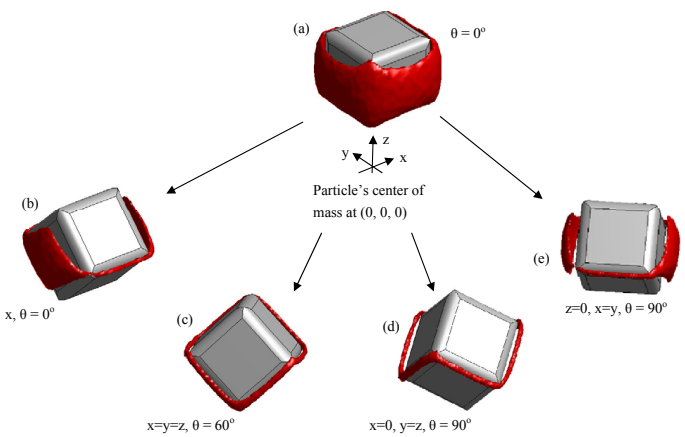

Fig. 8: 3D visualizations of NLC distortion around a cubic nanoparticle oriented at $\theta = 0°$, and at zero torque configuration along the four symmetry axes considered in this study.

When a cubic particle orients with its four lateral faces parallel to the far field director $n(r)$ (i.e. out-of-plane orientations), the torque reaches maximum (see the blue region in Fig. 7, and 3D visualization of NLC distortion around the maximum torque configuration in Fig. 8(a)) since the NLC around the particle is highly distorted. The magnitude of the out-of-plane torques on either side of the stable configuration is similar (Fig. 7). In the case of a cubic particle oriented along the $z = 0$, $x = y$ axis, the stable configuration at $\theta \sim 55°$ is sandwiched between the out-of-plane torques (Fig. 7). Thus, the particle oriented at an out-of-plane configuration, with an angle of rotation greater than the stable configuration, would move away from that state

and reorient to the stable configuration at $\theta \sim 55°$, more quickly than that of a particle oriented with an angle of rotation smaller than the stable configuration, due to the larger slope (Fig. 7).

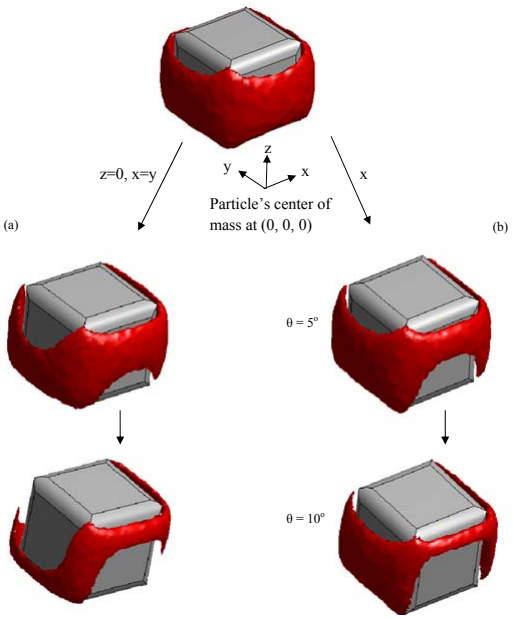

Fig. 9: 3D visualizations of NLC distortion around a cubic nanoparticle oriented at $\theta = 5°$ and $10°$, along (a) the axis $z = 0$, $x = y$ and (b) the x axis

3.2.3 Cubic particle rotated around x axis

When a cubic particle is rotated around the x axis, the torque profile is divided into three parts: (1) Starting with the zero torque configuration, similar to the Section 3.2.1, we observed the in-plane torques, as the angle of rotation decreases to $30°$ (Fig. 7); (2) just as the angle of rotation further decreases from $\theta \sim 30°$ to $20°$, we observed the out-of-plane torques similar to the Section 3.2.1 (Fig. 7); (3) we also observed an unconventional torque similar to the Section 3.2.2, while the angle of rotation further decreases from $\theta \sim 15°$ to $0°$ (Fig. 7, the corresponding 3D visualization in Fig. 9(b) and refer [21]). A cubic particle oriented along the x axis has both the most stable and a zero torque configuration at $\theta = 45°$ (Fig. 7 and 8(b)). When a cubic particle orients with its four lateral faces parallel to the far field director $n(r)$ (i.e. out-of-plane orientations), the torque reaches maximum (see the blue region in Fig. 7, and 3D visualization of NLC distortion around the maximum torque configuration in Fig. 8(a)) since the NLC around the particle is highly distorted. The magnitude of the in-plane torque is similar to that of the out-of-plane torque (Fig. 7). When a cubic particle is oriented around the x axis, the out-of-plane torque varies more with the angle of rotation than the in-plane torque, because of the larger slope (Fig. 7). Therefore, a cubic particle oriented at the unstable configuration (out-of-plane orientations), along the x axis, moves away immediately from that state and then slowly reorients itself to the stable configuration (in-plane orientations).

3.2.4 Comparisons

When a particle is oriented at the unstable (out-of-plane) configuration, the total torque (in-plane and out-of-plane) transmitted by the NLC to the particle in order to reorient it to the stable (in-plane) configuration depends on the difference in the NLC distortion around the most unstable and the most stable configuration. If the difference in the NLC distortion is large, then the higher torques is transmitted by the NLC to the particle due to the stronger driving force and vice versa. PMF value represents the stability of a particular orientation (i.e. the NLC distortion). The total torque transmitted by the NLC on a cubic particle rotated around the x-axis,

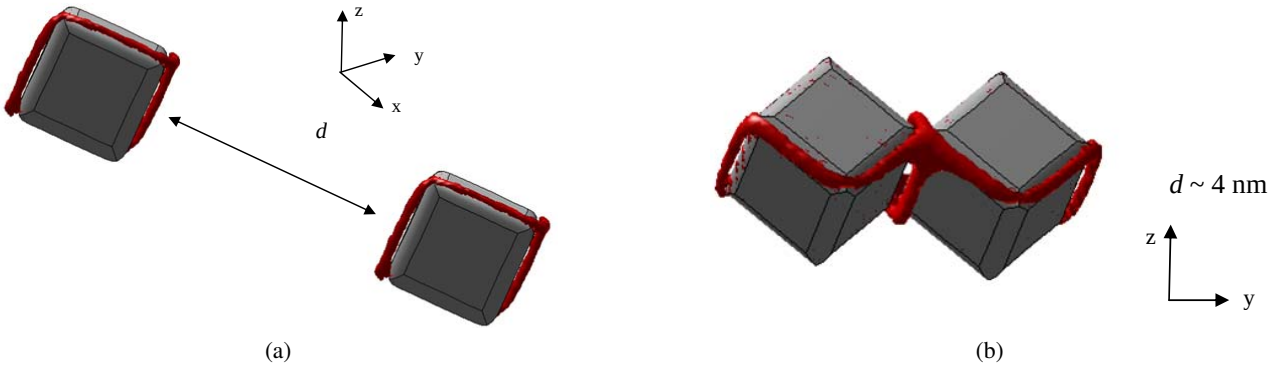

Fig. 10: (a) Schematic representation of two cubic particles approaching each other through the interparticle distance d. (b) 3D visualization of NLC distortion around two cubic particles separated by the interparticle distance $d \sim 4$ nm.

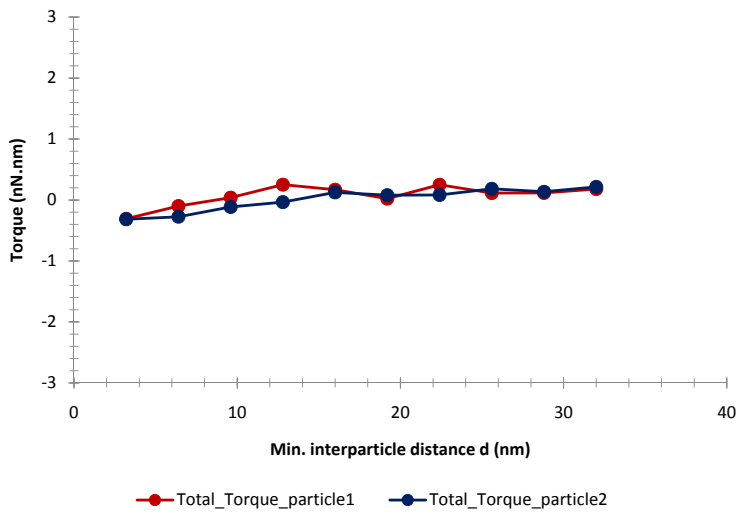

Fig. 11: Total torque transmitted by nematic liquid crystal on two cubic particle system as a function of minimum surface-to-surface interparticle distance d. Circles: total torque acting over particle 1 (red) and 2 (blue).

is nearly four times lower than that on a cubic particle rotated around all the other axes (Fig. 7). This is the axis of rotation effect because, when the particle is rotated around the x-axis only, the difference in the NLC distortion ($\sim$ 35 kBt) around the most unstable (out-of-plane) and the most stable (in-plane) configuration is smaller than that of a particle rotated around all the other axes ($\sim$ 125 kBt)[21]. Hence, the lower torques are transmitted by the NLC on a cubic particle rotated around the x-axis than all the other axes.

The torque transmitted by the NLC on a triangular prism shaped particle (Fig. 3) is nearly twice than that on a cubic particle (Fig. 7). This is a size effect because, in our work, a triangular prism particle has more surface area than that of a cubic particle. Thus, the NLC distortion at the most unstable configuration for a triangular prism particle ($\sim$ 185 kBt) is higher than that for a cubic particle (125 kBt)[21]. The difference in the NLC distortion around the most unstable and the most stable configuration is larger for a triangular prism ($\sim$ 185 kBt) particle than a cubic particle ($\sim$ 125 kBt)[21]. Hence, the higher torques are transmitted by the NLC on a triangular prism shaped particle. This demonstrates that, under the possible switching condition, with the ratio of the size of nanocube to nanoprism similar to this work, a stronger driving force is required to reorient the triangular prism shaped particles back to the stable configuration as compared to the cubic particles.

3.2.5 Two cubic particle system

For the two cubic particle systems, the torques were calculated, while the two particles approach each other, with each particle having fixed orientations equal to the thermodynamically stable configuration obtained from the one particle system (Fig. 10(a)). Since, according to our previous work for the PMF and the defect structures[21], several one-particle configurations had the similar thermodynamic stability, a configuration, where the cubic nanoparticle is rotated around the $x = y = z$ axes at an angle $\theta = 600$, is used for the two particle systems. We allowed two cubic particles approach in such a way that the defects touch each other and their respective rounded edges are parallel to each other (Fig. 10(a)). Our results indicate that there is no significant variation in all the three components of the torque transmitted by the NLC to the cubic nanoparticles approaching each other along the $x - y$ plane. Therefore, the total torque acting on both the cubic nanoparticles is presented in Fig. 11.

The total torque transmitted by the NLC, on both the cubic nanoparticles, is ~ 0 nN.nm for the entire interparticle distances considered as shown in the Fig. 11. This behavior is observed because both the particles approach with their edges parallel to each other and each particle is oriented around the $x = y = z$ axes at an angle $\theta = 600$, which has a zero torque. When the particles are close to each other, the total torque on each triangular prism shaped particle (~ 3.5 nN.nm) is higher than that on a cubic particle (~ 0 nN.nm) (Fig. 5 and 11), due to the presence of their respective particle. This difference is the result of the fact that the triangular prism particles approach with their rectangular faces parallel to each other whereas the cubic particles approach with their edges parallel to each other (Fig. 6(a) and 10(b)).

4 Concluding remarks

We investigated the torques transmitted by the NLC to the faceted particle, namely cubic and equilateral triangular prism shaped particle, in order to analyze the reorientational behavior of a faceted particle to the stable (minimum distortion) configuration. For the one particle system, the torque profile was mainly divided into two parts: (1) the in-plane torques and (2) the out-of-plane torques, except when a cubic particle was oriented along the $z = 0$, $x = y$ axis, where the torque profile has only the out-of-plane torques. The magnitude of the out-of-plane torque is similar to that of the in-plane torque, but their variation with respect to the angle of rotation differs. Mostly, the out-of-plane torque varies more than the in-plane torques, with respect to the angle of rotation, due to their large slope. These out-of-plane orientations are unstable configurations and when a particle is oriented at these configurations, it immediately moves away from that state, which is evident by the large slope, and then it slowly reorients itself to the closest stable configuration. In the torque profile, generally, the stable configuration also has a zero torque except when a cubic particle was oriented along $z = 0$, $x = y$ axis. In order to have a zero torque, a configuration should have a high degree of symmetry along with a low surface area of NLC distortion around it.

In the case of an equilateral triangular prism shaped particle system, the torque reaches maximum when the particle orients with one of its rectangular sides parallel to the far field director $n(r)$ (i.e. out-of-plane orientations). Whereas, in the case of a cubic particle, the torque reaches maximum when the particle orients with its four lateral faces parallel to the far field director $n(r)$ (i.e. out-of-plane orientations). Our results suggests that the torque transmitted by the NLC on a cubic particle rotated around the x-axis (Fig. 7), is nearly five times lower than that on a cubic particle rotated around all the other axes (Fig. 7), because of the axis of rotation affect. Our results also indicate that, due to the size effect, the torque transmitted by the NLC on a triangular prism shaped particle (Fig. 3) is nearly twice than that on a cubic particle (Fig. 7). Thus, under the possible switching condition, with the ratio of size of nanocube to nanoprism similar to our work, a stronger driving force is required to reorient the triangular prism shaped particles back to their stable configurations as compared to the cubic particles.

For the two-particle systems, it is observed that, when the two particles are close to each other, the NLC transmits more torque on a stable triangular nanoprism than that on a stable nanocube, as a result of the presence of their respective particle (Fig. 5 and 11). This difference in the magnitude of the total torque is because of the difference in their trajectory of approach (Fig. 6(a) and 10(b)). It is known that the magnitude of

the torques on the particles can be reduced to some extent by allowing them approach each other via 'diagonal' trajectory. Due to the non-spherical shape of the particles, the nematic LC is also expected to transmit force on the particles. Calculation of the forces is not considered in this work and would be the subject of future studies.

References

[1] A. N. Beris. *Thermodynamics of Flowing Systems with Internal Microstructure*. Oxford University Press, New York, 1994.

[2] A. C. Callan-Jones, R. A. Pelcovits, et al. Simulation and visualization of topological defects in nematic liquid crystals. *Physical Review E - Statistical, Nonlinear, and Soft Matter Physics*, 2006, **74**: 061701.

[3] K.-S. Cho, D. V. Talapin, et al. Designing pbse nanowires and nanorings through oriented attachment of nanoparticles. *Journal of the American Chemical Society*, 2005, **127**: 40–47.

[4] COMSOL. Comsol multiphysicstm version 3.4 user's guide, 2007.

[5] P. G. de Gennes, J. Prost. *The Physics of Liquid Crystals, Second Edition*. Oxford University Press, New York, 1993.

[6] D. Dendukuri, D. C. Pregibon, et al. Continuous-flow lithography for high-throughput microparticle synthesis. *Nature Materials*, 2006, **5**: 365–369.

[7] der Schoot Paul van, V. Popa-Nita, S. Kralj. Alignment of carbon nanotubes in nematic liquid crystals. *Journal of Physical Chemistry B*, 2008, **112**: 4512–4518.

[8] I. Dierking, G. Scalia, et al. Aligning and reorienting carbon nanotubes with nematic liquid crystals. *Advanced Materials*, 2004, **16**: 865–869.

[9] J. Dontabhaktuni, M. Ravnik, S. Zumer. Shape-tuning the colloidal assemblies in nematic liquid crystals. *Soft Matter*, 2012, **8**: 1657–1663.

[10] B. J. Edwards, A. N. Beris. Order parameter representation of spatial inhomogeneities in polymeric liquid crystals. *J. Rheol. (N. Y.)*, 1989, **33**: 1189–1193.

[11] B. J. Edwards, A. N. Beris, M. Grmela. Generalized constitutive equation for polymeric liquid crystals. part 1. model formulation using the hamiltonian (poisson bracket) formulation. *Journal of Non-Newtonian Fluid Mech*, 1990, **35**: 51–72.

[12] S. Gangwal, O. J. Cayre, O. D. Velev. Dielectrophoretic assembly of metallodielectric janus particles in ac electric fields. *Langmuir*, 2008, **24**: 13312–13320.

[13] S. C. Glotzer. Materials science: Some assembly required. *Science (Washington, DC, U. S.)*, 2004, **306**: 419–420.

[14] S. C. Glotzer, M. J. Solomon. Anisotropy of building blocks and their assembly into complex structures. *Nature Materials*, 2007, **6**: 557–562.

[15] S. Grollau, E. B. Kim, et al. Monte carlo simulations and dynamic field theory for suspended particles in liquid crystalline systems. *Journal of Chemical Physics*, 2003, **119**: 2444–2455.

[16] V. K. Gupta, N. L. Abbott. Design of surfaces for patterned alignment of liquid crystals on planar and curved substrates. *Science (Washington, D. C.)*, 1997, **276**: 1533–1536.

[17] O. Guzman, N. L. Abbott, P. J. J. De. Defect structures and three-body potential of the mean force for nanoparticles in a nematic host. *Journal of Polymer Science Part B: Polymer Physics*, 2005, **43**: 1033–1040.

[18] O. Guzman, S. G. E. B. Kim, et al. Defect structure around two colloids in a liquid crystal. *Physical Review Letters*, 2003, **91**: 235507.

[19] T. Hegmann, H. Qi, V. M. Marx. Nanoparticles in liquid crystals: Synthesis, self-assembly, defect formation and potential applications. *Journal of Inorganic and Organometallic Polymers and Materials*, 2007, **17**: 483–508.

[20] F. R. Hung. Quadrupolar particles in a nematic liquid crystal: Effects of particle size and shape. *Physical Review E: Statistical, Nonlinear, and Soft Matter Physics* , 2009, **79**: 1–11.

[21] F. R. Hung, S. Bale. Faceted nanoparticles in a nematic liquid crystal: Defect structures and potentials of mean force. *Molecular Simulation*, 2009, **35**.

[22] F. R. Hung, B. T. Gettelfinger, et al. Nanoparticles in nematic liquid crystals: Interactions with nanochannels. *Journal of Chemical Physics*, 2007, **127**: 1–10.

[23] F. R. Hung, O. Guzman. Anisotropic nanoparticles immersed in a nematic liquid crystal: Defect structures and potentials of mean force. *Physical Review E: Statistical, Nonlinear, and Soft Matter Physics* , 2006, **74**: 1–12.

[24] J. ichi Fukuda, M. Yoneya, H. Yokoyama. Nematic liquid crystal around a spherical particle: Investigation of the defect structure and its stability using adaptive mesh refinement. *European Physical Journal E*, 2004, **13**: 87–98.

[25] A. M. Kalsin, M. Fialkowski, et al. Electrostatic self-assembly of binary nanoparticle crystals with a diamond-like lattice. *Science (Washington, DC, U. S.)*, 2006, **312**.

[26] E. B. Kim, O. Guzman, et al. Interactions between spherical colloids mediated by a liquid crystal: A molecular simulation and mesoscale study. *Journal of Chemical Physics*, 2004, **121**: 1949–1961.
[27] K. Kita, M. Ichikawa, Y. Kimura. Self-assembly of polymer droplets in a nematic liquid crystal at phase separation. *Physical Review E: Statistical, Nonlinear, and Soft Matter Physics*, 2008, **77**: 1–4.
[28] P. A. Kossyrev, A. Yin. Electric field tuning of plasmonic response of nanodot array in liquid crystal matrix. *Nano Letters*, 2005, **5**: 1978–1981.
[29] S. Kralj, E. G. Virga. Core hysteresis in nematic defects. *Physical Review E: Statistical, Nonlinear, and Soft Matter Physics*, 2002, **66**: 021703.
[30] S. Kralj, E. G. Virga, S. Zumer. Biaxial torus around nematic point defects. *Physical Review E: Statistical, Nonlinear, and Soft Matter Physics*, 1999, **60**: 1858–1866.
[31] C. Lapointe, A. Hultgren. Elastic torque and the levitation of metal wires by a nematic liquid crystal. *Science (Washington, DC, U. S.)*, 2004, **30**: 652–655.
[32] C. P. Lapointe, S. Hopkins. Electrically driven multiaxis rotational dynamics of colloidal platelets in nematic liquid crystals. *Physical Review Letters*, 2010, **105**: 1–4.
[33] J.-C. Loudet, P. Barois, P. Poulin. Colloidal ordering from phase separation in a liquid-crystalline continuous phase. *Nature (London)*, 2000, **407**: 611–613.
[34] M. D. Lynch, D. L. Patrick. Organizing carbon nanotubes with liquid crystals. *Nano Letters*, 2002, **2**: 1197–1201.
[35] M. D. Lynch, D. L. Patrick. Controlling the orientation of micron-sized rod-shaped sic particles with nematic liquid crystal solvents. *Chemistry of Materials*, 2004, **16**: 762–767.
[36] N. Malikova, I. Pastoriza-Santos. Layer-by-layer assembled mixed spherical and planar gold nanoparticles: Control of interparticle interactions. *Langmuir*, 2002, **18**: 3694–3697.
[37] G. McKay, E. G. Virga. Mechanical actions on nanocylinders in nematic liquid crystals. *Physical Review E: Statistical, Nonlinear, and Soft Matter Physics*, 2005, **71**: 1–11.
[38] M. Mitov, C. Bourgerette, G. F. De. Fingerprint patterning of solid nanoparticles embedded in a cholesteric liquid crystal. *Journal of Physics: Condensed Matter* , 2004, **16**: S1981–S1988.
[39] I. Musevic, M. Skarabot. Two-dimensional nematic colloidal crystals self-assembled by topological defects. *Science (Washington, DC, U. S.)*, 2006, **313**: 954–958.
[40] V. G. Nazarenko, A. B. Nych, B. I. Lev. Crystal structure in nematic emulsion. *Physical Review Letters*, 2001, **87**: 075504.
[41] S. R. Nersisyan, N. V. Tabiryan. The effect of low-frequency microvibrations on nanoparticle networks embedded in liquid crystals. *Physical Review Letters*, 2006, **88**: 1–3.
[42] A. B. Nych, U. M. Ognysta. Coexistence of two colloidal crystals at the nematic-liquid-crystal-air interface. *Physical Review Letters*, 2007, **98**: 057801.
[43] U. Ognysta, A. Nych. 2d interactions and binary crystals of dipolar and quadrupolar nematic colloids. *Physical Review Letters*, 2008, **100**: 217803.
[44] M. Petrov, B. Katranchev, et al. Optical properties of dimeric liquid crystals doped with single-walled carbon nanotubes. *Journal of Physics: Conference Series*, 2012, **398**: 1–6.
[45] P. M. Phillips, N. Mei, et al. Textures in polygonal arrangements of square nanoparticles in nematic liquid crystal matrices. *Langmuir,*, 2011, **27**: 13335–13341.
[46] P. Poulin, V. Cabuil, D. A. Weitz. Direct measurement of colloidal forces in an anisotropic solvent. *Physical Review Letters*, 1997, **79**: 4862–4865.
[47] P. Poulin, H. Stark. Novel colloidal interactions in anisotropic fluids. *Science*, 1997, **25**: 1770–1773.
[48] P. Poulin, D. A. Weitz. Inverted and multiple nematic emulsions. *Physical Review E: Statistical Physics, Plasmas, Fluids, and Related Interdisciplinary Topics*, 1998, **57**: 626–637.
[49] H. Qi, T. Hegmann. Formation of periodic stripe patterns in nematic liquid crystals doped with functionalized gold nanoparticles. *Journal of Materials Chemistry*, 2006, **16**: 4197–4205.
[50] H. Qi, T. Hegmann. Impact of nanoscale particles and carbon nanotubes on current and future generations of liquid crystal displays. *Journal of Materials Chemistry*, 2008, **18**: 3288–3294.
[51] H. Qi, A. Lepp, et al. Effects of hydrophilic and hydrophobic gold nanoclusters on the stability and ordering of bolaamphiphilic liquid crystals. *Journal of Materials Chemistry*, 2007, **17**: 2139–2144.
[52] M. Ravnik, M. Skarabot, et al. Entangled nematic colloidal dimers and wires. *Physical Review Letters*, 2007, **99**: 247801.
[53] J. B. Rovner, D. S. Borgnia. Elastic and hydrodynamic torques on a colloidal disk within a nematic liquid crystal. *Physical Review E: Statistical, Nonlinear, and Soft Matter Physics*, 2012, **86**: 1–9.
[54] B. Senyuk, I. I. Smalyukh. Elastic interactions between colloidal microspheres and elongated convex and concave nanoprisms in nematic liquid crystals. *Soft Matter*, 2012, **8**: 8729–8734.
[55] E. V. Shevchenko, D. V. Talapin. Structural diversity in binary nanoparticle superlattices. *Nature*, 2006, **439**: 55–59.

[56] M. Skarabot, M. Ravnik. Interactions of quadrupolar nematic colloids. *Physical Review E: Statistical, Nonlinear, and Soft Matter Physics*, 2008, **77**: 031705.
[57] M. Skarabot, M. Ravnik, et al. Hierarchical self-assembly of nematic colloidal superstructures. *Physical Review E: Statistical, Nonlinear, and Soft Matter Physics*, 2008, **77**: 061706.
[58] M. Skarabot, M. Ravnik, et al. Two-dimensional dipolar nematic colloidal crystals. *Physical Review E: Statistical, Nonlinear, and Soft Matter Physics*, 2008, **76**: 051406.
[59] I. I. Smalyukh, S. Chernyshuk, et al. Ordered droplet structures at the liquid crystal surface and elastic-capillary colloidal interactions. *Physical Review Letters*, 2004, **93**: 117801.
[60] K. J. Stebe, E. Lewandowski, M. Ghosh. Materials science. oriented assembly of metamaterials. *Science*, 2009, **325**: 159–160.
[61] Y. Sun, Y. Xia. Shape-controlled synthesis of gold and silver nanoparticles. *Science*, 2002, **298**: 2176–2179.
[62] K. Takahashi, M. Ichikawa, Y. Kimura. Force between colloidal particles in a nematic liquid crystal studied by optical tweezers. *Physical Review E: Statistical, Nonlinear, and Soft Matter Physics*, 2008, **77**: 1–4.
[63] Y. Tao, Y. H. Tam. Dynamics of zno nanowires immersed in in-plane switching liquid crystal cells. *Applied Physics Letters*, 2013, **103**: 1–4.
[64] U. Tkalec, M. Skarabot, I. Musevic. Interactions of micro-rods in a thin layer of a nematic liquid crystal. *Soft Matter*, 2008, **4**: 2402–2409.
[65] B. M. C. W. Van, R. H. C. Janssen, et al. Polymer-filled nematics: A new class of light-scattering materials for electro-optical switches. *Advanced Materials*, 2000, **12**: 753–757.
[66] O. D. Velev. Self-assembly of unusual nanoparticle crystals. *Science*, 2006, **312**: 376–377.
[67] M. Yada, J. Yamamoto, H. Yokoyama. Spontaneous formation of regular defect array in water-in-cholesteric liquid crystal emulsions. *Langmuir*, 2002, **18**: 7436–7440.
[68] M. Yada, J. Yamamoto, H. Yokoyama. Direct observation of anisotropic interparticle forces in nematic colloids with optical tweezers. *Physical Review Letters*, 2004, **92**: 1–4.